Correlation effects on magnetic frustration in the triangular-lattice Hubbard model

Saptarshi Ghosh* and Avinash Singh
Department of Physics, Indian Institute of Technology, Kanpur-208016, India
(Received 1 October 2007; published 26 March 2008)

Evolution of the magnetic response function in the triangular-lattice Hubbard model is studied, with interaction strength within a systematic inverse-degeneracy expansion scheme which incorporates self-energy and vertex corrections and explicitly preserves the spin-rotation symmetry. It is shown that at half-filling, the response function goes through a nearly dispersionless regime around the K point for intermediate coupling strength, before undergoing an inversion at strong coupling, resulting in maximum response at K, consistent with the expected 120° antiferromagnetic instability. Effects of finite hole and electron doping on the magnetic response function are also examined.

DOI: 10.1103/PhysRevB.77.094430 PACS number(s): 75.30.Ds, 71.27.+a, 71.10.Fd

I. INTRODUCTION

There has been renewed interest in correlated electron systems on triangular lattices, as evidenced by recent studies of antiferromagnetism, superconductivity, and metal-insulator transition in the organic systems κ-(BEDT-TTF)$_2X$,[1,2] the discovery of superconductivity in $Na_xCoO_{2\cdot y}H_2O$,[3] the observation of low-temperature insulating phases in some $\sqrt{3}$-adlayer structures such as potassium on Si[111],[4] and quasi-two-dimensional 120° spin ordering and spin-wave excitations in $RbFe(MoO_4)_2$ (Refs. 5 and 6) and the multiferroic materials $YMnO_3$ and $HoMnO_3$.[7–10]

Transverse spin fluctuations in the 120°-ordered antiferromagnetic (AF) state of the triangular-lattice Hubbard model at half-filling were recently investigated in the full range of interaction strength U.[11,12] While a stable AF state was obtained in the strong-coupling limit, with identical spin-wave dispersion as for the equivalent quantum Heisenberg antiferromagnet (QHAF), with decreasing U the spin stiffness was found to vanish at $U/t \approx 6$. In addition, the magnon energy ω_M at the M point in the Brillouin zone was found to vanish at $U/t \approx 7$, with the magnon amplitudes indicating instability of the AF state with respect to out-of-plane fluctuations. The loss of magnetic order due to divergent quantum fluctuations yields a magnetic phase transition to a quantum spin-disordered insulator, which is relevant to the spin-liquid state and Mott transition in the organic systems κ-(BEDT-TTF)$_2X$. The existence of stable 120° AF ordering at large U but vanishing spin stiffness and ω_M at finite U implies that the triangular-lattice Hubbard model exhibits, besides the intrinsic geometrical frustration of the triangular lattice, an additional U-controlled frustration due to competing extended-range spin couplings generated at finite U.

In view of this enhanced magnetic frustration in the triangular-lattice Hubbard model at finite U, it is, therefore, of interest to examine how the magnetic response function evolves with increasing interaction strength in the correlated paramagnetic (PM) state. Even at the bare level, the magnetic response function shows very rich behavior (Fig. 1). The comparable magnetic response at different symmetry points in the Brillouin zone, corresponding to very different magnetic orderings, represents the weak-coupling picture of competing orders and magnetic frustration in the triangular-lattice paramagnet. Furthermore, the bare response is not maximum at the K point corresponding to 120° AF ordering. In view of the expected instability toward the 120° AF ordering at strong coupling, it would be desirable to develop an approach wherein the evolution of the magnetic response with increasing interaction strength U is consistent with this AF instability.

Given that the 120° AF state is stable in the strong-coupling limit, it would be desirable to use a many-body approach which continuously interpolates to the spontaneously-broken-symmetry AF state and yields a proper description of the Goldstone mode and spin waves by preserving the spin-rotation symmetry. From this viewpoint,

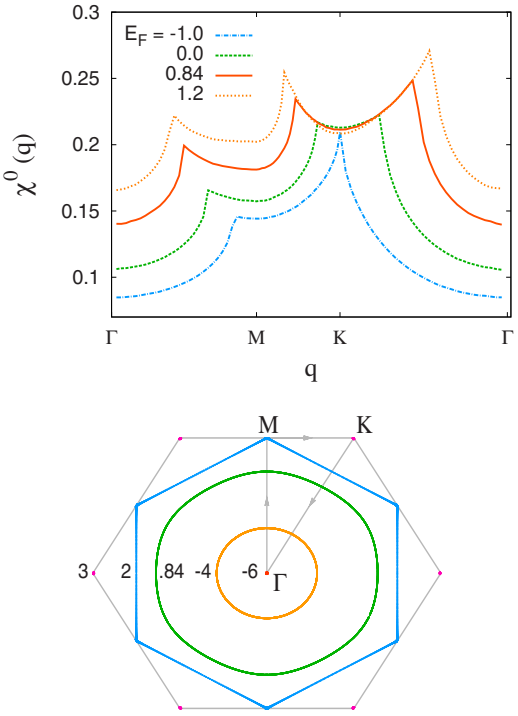

FIG. 1. (Color online) The bare magnetic response function at different fillings, showing the relative suppression (enhancement) of the K response (which corresponds to 120° AF ordering) with electron (hole) doping. Also shown are few constant-energy contours in the triangular-lattice Brillouin zone.

evaluating many-body corrections reliably in the intermediate- and strong-coupling regimes remains a challenge. Schemes such as the dynamical mean-field theory and fluctuation-exchange approximation, although providing powerful tools for studying the correlated paramagnet, do not continue into the broken-symmetry state without breaking the essential spin-rotation symmetry of the Hamiltonian as the Goldstone mode is not preserved, while the two-particle self-consistent (TPSC) approximation does not renormalize the momentum structure of the magnetic response function.

In this paper, we will use a systematic many-body expansion scheme to investigate the momentum-dependent magnetic response function, and study its evolution with increasing interaction strength. For this purpose, we will use a systematic inverse-degeneracy $(1/\mathcal{N})$ expansion scheme which explicitly preserves the spin-rotational symmetry by including self-energy diagrams as well as the corresponding vertex corrections. The importance of including vertex corrections in preserving spin-rotation symmetry has been highlighted in the context of paramagnon corrections[13] in He^3 the AF ground state,[14] and the ferromagnetic ground state.[15,16] Indeed, we will show that the dominant quantum correction to the response function arises from the vertex corrections, signifying suppression due to particle-particle correlations. Therefore, from the paramagnetic side, vertex corrections play a dominant role in suppressing magnetic frustration and stabilizing the 120° AF ordering at half-filling.

The Hubbard model on a triangular lattice has been studied recently using a variety of tools. The zero-temperature phase diagram has been studied using the slave boson (SB) technique and the exact diagonalization.[17,18] The mean-field SB approach yields a rich phase diagram qualitatively resembling the Hartree-Fock (HF) results.[19,20] The nonmagnetic insulating (NMI) state near the Mott transition has been studied using the path integral renormalization group (PIRG) method,[21] in which the HF results are systematically improved to reach the true ground state by taking account of quantum fluctuations. Results show a generic emergence of a NMI state sandwiched by a Mott metal-insulator transition and an AF transition. One-electron density of states has been examined using the quantum Monte Carlo method,[22] showing a pseudogap development for intermediate U, accompanied by two peaks in the spin structure factor, signaling the formation of a spiral spin density wave. A weak-coupling renormalization group analysis applied to the anisotropic triangular lattice shows that frustration suppresses the AF instability in favor of a superconducting instability.[23] A magnetic field induced exotic spin-triplet superconductivity has been proposed, having strong ferromagnetic fluctuations.[24]

A spin-liquid type NMI state sandwiched between a weak-coupling PM state and a strong-coupling antiferromagnetic insulator state has also been obtained for the t-t'–Hubbard model on a square lattice and an anisotropic triangular lattice using the PIRG method.[25,26] The NMI state has been recently suggested to be a new type of degenerate quantum spin phase having gapless and dispersionless spin excitations.[26] At the same time, this result of an intervening NMI state is in contradiction to the earlier finding of an intermediate metallic AF state.[27] In the context of κ-$(BEDT\text{-}TTF)_2Cu_2(CN)_3$, spin-liquid phases near the Mott transition in the Hubbard model have also been studied within the U(1) gauge theory.[28]

The organization of the paper is as follows. The inverse-degeneracy expansion scheme is briefly reviewed in Sec. II. The order-$1/\mathcal{N}$ diagrams for the irreducible propagator and their expressions are given in Sec. III. Results at half-filling and for finite electron and hole doping are discussed in Secs. IV and V, and conclusions are presented in Sec. VI. Evaluation of the fermion vertices by integrating out the fermion energy-momentum degrees of freedom is illustrated in Appendix A. Emergence of the pseudogap in the one-electron density of states due to order-$1/\mathcal{N}$ self-energy corrections is discussed in Appendix B.

II. INVERSE-DEGENERACY EXPANSION

We consider the generalized $\mathcal{N}$-orbital Hubbard model:[14]

$$H = -t \sum_{\langle ij\rangle,\sigma,\alpha} (a^\dagger_{i\sigma\alpha} a_{j\sigma\alpha} + \text{H.c.}) + \frac{1}{\mathcal{N}} \sum_{i,\alpha,\beta} (U_1 a^\dagger_{i\uparrow\alpha} a_{i\uparrow\alpha} a^\dagger_{i\downarrow\beta} a_{i\downarrow\beta} + U_2 a^\dagger_{i\uparrow\alpha} a_{i\uparrow\beta} a^\dagger_{i\downarrow\beta} a_{i\downarrow\alpha}), \tag{1}$$

where α, β refer to the degenerate orbital indices and the factor $1/\mathcal{N}$ is included to render the energy density finite in the $\mathcal{N}\to\infty$ limit. In the isotropic limit $(U_1 = U_2 = U)$, the two interaction terms (density-density and exchange type with respect to orbital indices) are together equal to $U(-\mathbf{S}_i \cdot \mathbf{S}_i + n_i^2)$ in terms of the total spin $\mathbf{S}_i \equiv \Sigma_\alpha \psi^\dagger_{i\alpha}(\boldsymbol{\sigma}/2)\psi_{i\alpha}$ and charge $n_i \equiv \Sigma_\alpha \psi^\dagger_{i\alpha}(1/2)\psi_{i\alpha}$ operators, and the Hamiltonian is, therefore, explicitly spin-rotationally symmetric.

With z as the spin-quantization direction, it is convenient to evaluate the time-ordered transverse spin-fluctuation propagator:

$$\chi^{-+}(\mathbf{q},\omega) = i \int dt e^{i\omega(t-t')} \sum_\beta \sum_j e^{i\mathbf{q}\cdot(\mathbf{r}_i - \mathbf{r}_j)} \times \langle \Psi_0 | \mathrm{T}[S^-_{i\alpha}(t) S^+_{j\beta}(t')] \Psi_0 \rangle \tag{2}$$

involving the spin-lowering and spin-raising operators $S^\mp = \psi^\dagger(\sigma^\mp/2)\psi$, where ψ is the electron field operator. The transverse propagators χ^{-+} and χ^{+-} yield the x, y components of the magnetic response, which are identical to the z response due to spin isotropy in the PM ground state $|\Psi_0\rangle$. When evaluated in the spontaneously-broken-symmetry state, the transverse spin-fluctuation propagator also describes collective spin-wave and particle-hole Stoner excitations.[11,12]

In terms of the exact irreducible propagator $\phi(\mathbf{q},\omega)$, which incorporates all self-energy and vertex corrections, the spin-fluctuation propagator can be generally expressed as

$$\chi^{-+}(\mathbf{q},\omega) = \frac{\phi(\mathbf{q},\omega)}{1 - U\phi(\mathbf{q},\omega)}. \tag{3}$$

The inverse-degeneracy expansion[14]

$$\phi = \phi^{(0)} + \left(\frac{1}{\mathcal{N}}\right)\phi^{(1)} + \left(\frac{1}{\mathcal{N}}\right)^2 \phi^{(2)} + \cdots \tag{4}$$

systematizes the diagrams for ϕ in powers of the expansion parameter $1/\mathcal{N}$ which, in analogy with $1/S$ for quantum spin systems, plays the role of $\hbar$. This expansion explicitly preserves spin-rotational symmetry and, therefore, the Goldstone mode in the broken-symmetry state, and has been used recently to evaluate quantum corrections to spin-wave energies and spin stiffness in the antiferromagnetic[14] and ferromagnetic[16] states of the Hubbard model.

$\mathcal{N}\to\infty$ limit

In the $\mathcal{N}\to\infty$ limit, only the "classical" term $\phi^{(0)}\equiv\chi^0$ survives, and the ladder series with interaction U_2 yields the random phase approximation (RPA):

$$\chi^{-+}_{\mathrm{RPA}}(\mathbf{q},\omega) = \frac{\chi^0(\mathbf{q},\omega)}{1 - U\chi^0(\mathbf{q},\omega)}, \tag{5}$$

amounting to a classical description of noninteracting spin-fluctuation modes. Here, the bare antiparallel-spin particle-hole propagator:

$$\phi^{(0)}(\mathbf{q},\omega) \equiv \chi^0(\mathbf{q},\omega) = \sum_{\mathbf{k}} \left(\frac{1}{\epsilon^{\uparrow +}_{\mathbf{k}} - \epsilon^{\downarrow -}_{\mathbf{k}-\mathbf{q}} - \omega - i\eta} + \frac{1}{\epsilon^{\downarrow +}_{\mathbf{k}-\mathbf{q}} - \epsilon^{\uparrow -}_{\mathbf{k}} + \omega - i\eta} \right), \tag{6}$$

where $\epsilon^{\sigma}_{\mathbf{k}} = \epsilon_{\mathbf{k}} + (U_1 n/2)$ are the HF band energies in the PM state, and the superscript $+$ $(-)$ refers to particle (hole) states above (below) the Fermi energy E_F. The spin-independent HF band-energy shift $U_1 n/2$, corresponding to the $\mathcal{N}\to\infty$ self-energy, can be trivially transformed away by an energy shift, as assumed henceforth.

The bare particle-hole propagator $\chi^0(\mathbf{q})$ yields the magnetic response to a static, spatially varying magnetic field, the rich behavior of which is shown in Fig. 1 for different Fermi energies, with corresponding fillings $n=0.6$, 0.8, 1.0, and 1.1, respectively. Also shown are few constant-energy contours in the triangular-lattice Brillouin zone. Contributions to χ^0 from particle states near the nested hexagonal contour $(\epsilon_{\mathbf{k}}=2)$ with divergent density of states are responsible for the cusps in the bare magnetic response function. For half-filling, the most significant features are the comparable response at the three symmetry points Γ, M, and K, and peaks at the three points approximately midway between them. The magnetic orderings corresponding to the three symmetry points Γ, M, and K are (0,0,0), $(0,\pi,\pi)$, and $(2\pi/3,2\pi/3,2\pi/3)$, respectively, where the triplet corresponds to the ordering wave vector in the three lattice directions. Similarly, for the three midpoints $M/2$, $(M+K)/2$, and $3K/4$, the ordering wave vectors are $(0,\pi/4,\pi/4)$, $(\pi/6,7\pi/6,7\pi/6)$, and $(\pi,\pi/4,\pi/4)$, respectively.

The comparable magnetic response at these six symmetry points, which correspond to very different magnetic orderings, represents the weak-coupling picture of competing orders and magnetic frustration in the triangular-lattice paramagnet. Note that the response at K, corresponding to 120° ordering, is not maximum. In view of the expected instability toward 120° AF ordering at strong coupling, it is of particular interest to examine the evolution of the magnetic response with increasing interaction U.

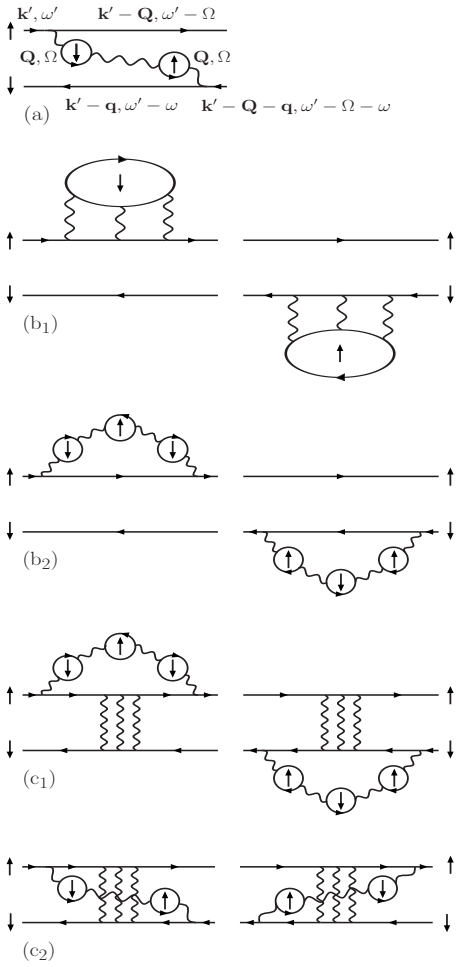

FIG. 2. The first-order quantum corrections to the irreducible particle-hole propagator $\phi(\mathbf{q},\omega)$.

III. $1/\mathcal{N}$ CORRECTIONS

The order-$1/\mathcal{N}$ diagrams which yield quantum correction $\phi^{(1)}$ to the irreducible particle-hole propagator $\phi(\mathbf{q},\omega)$ are shown in Fig. 2. The fermion lines represent the HF Green's functions G^0. Figures 2(b_1) and 2(b_2) incorporate self-energy corrections due to transverse and longitudinal spin fluctuations, involving ladders and bubbles with interactions U_2 and U_1, respectively. In these diagrams, each particle-hole pair of fermion lines in the ladder or bubble involves an orbital degree of freedom. Hence, a term with n interaction lines involves $n-1$ orbital summations, leaving a net factor of $1/\mathcal{N}$. Other self-energy diagrams with $1/\mathcal{N}$ corrections to the Hartree self-energy, as in the AF state, vanish identically as there are no quantum corrections to particle densities n_σ in the PM state. Figures 2(a). 2(c_1), and 2(c_2) involve vertex corrections, with Figs. 2(c_1) and 2(c_2) representing coupling of longitudinal and transverse spin fluctuations.

The quantum corrections represented by Figs. 2(a)–2(c) incorporate different aspects of correlation effects. These include renormalized and dynamical effective interactions [Fig. 2(a)], negative correction due to spectral-weight transfer and energy renormalization arising from self-energy corrections [Figs. $2(b_1)$ and $2(b_2)$], and negative contribution due to particle-particle correlations of the crossed diagrams [Fig. $2(c_2)$]. The strong particle-particle correlations found in this study, which suppress the magnetic response through the vertex corrections, are relevant for pairing correlations in the context of the observed superconductivity in the BEDT compounds.

The corresponding expressions are given below. For Fig. 2(a), we obtain

$$\phi^{(a)}(\mathbf{q},\omega) = i\int_{-\infty}^{\infty}\frac{d\Omega}{2\pi}\sum_{\mathbf{Q}}\gamma^{(a)}(\mathbf{Q},\Omega)U_{\text{eff}}^{\uparrow\downarrow}(\mathbf{Q},\Omega), \tag{7}$$

where the four-fermion vertex

$$\gamma^{(a)}(\mathbf{Q},\Omega) = i\int\frac{d\omega'}{2\pi}\sum_{\mathbf{k}'}G^0(\mathbf{k}',\omega')G^0(\mathbf{k}'-\mathbf{q},\omega'-\omega)G^0(\mathbf{k}'-\mathbf{Q},\omega'-\Omega)G^0(\mathbf{k}'-\mathbf{Q}-\mathbf{q},\omega'-\Omega-\omega), \tag{8}$$

and the effective antiparallel-spin interaction

$$U_{\text{eff}}^{\uparrow\downarrow}(\mathbf{Q},\Omega) = \frac{U^3\chi_0^2(\mathbf{Q},\Omega)}{1-U^2\chi_0^2(\mathbf{Q},\Omega)} \tag{9}$$

involve the even-bubble series with interaction U_1.

For Figs. $2(b_1)$ and $2(b_2)$ involving self-energy corrections, we obtain

$$\phi^{(b)}(\mathbf{q},\omega) = -i\int_{-\infty}^{\infty}\frac{d\Omega}{2\pi}\sum_{\mathbf{Q}}\gamma^{(b)}(\mathbf{Q},\Omega)U_{\text{eff}}^{(b)}(\mathbf{Q},\Omega), \tag{10}$$

where the four-fermion vertex

$$\gamma^{(b)}(\mathbf{Q},\Omega) = i\int_{-\infty}^{\infty}\frac{d\omega'}{2\pi}\sum_{\mathbf{k}'}[G^0(\mathbf{k}',\omega')]^2G^0(\mathbf{k}'-\mathbf{Q},\omega'-\Omega)\times[G^0(\mathbf{k}'-\mathbf{q},\omega'-\omega)+G^0(\mathbf{k}'+\mathbf{q},\omega'+\omega)] \tag{11}$$

and the effective interaction

$$U_{\text{eff}}^{(b)}(\mathbf{Q},\Omega) = \frac{U^2\chi_0(\mathbf{Q},\Omega)}{1-U\chi_0(\mathbf{Q},\Omega)} + \frac{U^2\chi_0(\mathbf{Q},\Omega)}{1-U^2\chi_0^2(\mathbf{Q},\Omega)} \equiv U_{\text{eff}}^{-+}(\mathbf{Q},\Omega) + U_{\text{eff}}^{\sigma\sigma}(\mathbf{Q},\Omega)$$

include the transverse contribution $U_{\text{eff}}^{-+}(\mathbf{Q},\Omega)$, involving the RPA ladder series (with interaction U_2), and the parallel-spin contribution $U_{\text{eff}}^{\sigma\sigma}(\mathbf{Q},\Omega)$, involving the RPA odd-bubble series (with interaction U_1).

Finally, for the vertex correction diagrams [Figs. $2(c_1)$ and $2(c_2)$], involving both the ladder series (with interaction U_2) and the bubble series (with interaction U_1), we obtain

$$\phi^{(c_1)}(\mathbf{q},\omega) = -i\int_{-\infty}^{\infty}\frac{d\Omega}{2\pi}\sum_{\mathbf{Q}}[\gamma^{(c)+}(\mathbf{Q},\Omega)\gamma^{(c)+}(\mathbf{Q},\Omega) + \gamma^{(c)-}(\mathbf{Q},\Omega)\gamma^{(c)-}(\mathbf{Q},\Omega)]\left(\frac{U}{1-U\chi_0(\mathbf{Q},\Omega)}\right)\times\left(\frac{U^2\chi_0(\mathbf{q}-\mathbf{Q},\omega-\Omega)}{1-U^2\chi_0^2(\mathbf{q}-\mathbf{Q},\omega-\Omega)}\right), \tag{12}$$

$$\phi^{(c_2)}(\mathbf{q},\omega) = +i\int_{-\infty}^{\infty}\frac{d\Omega}{2\pi}\sum_{\mathbf{Q}}2\gamma^{(c)+}(\mathbf{Q},\Omega)\gamma^{(c)-}(\mathbf{Q},\Omega)\times\left(\frac{U}{1-U\chi_0(\mathbf{Q},\Omega)}\right)\left(\frac{U}{1-U^2\chi_0^2(\mathbf{q}-\mathbf{Q},\omega-\Omega)}\right), \tag{13}$$

where the three-fermion vertices

$$\gamma^{(c)\pm}(\mathbf{Q},\Omega) = i\int_{-\infty}^{\infty}\frac{d\omega'}{2\pi}\sum_{\mathbf{k}'}G^0(\mathbf{k}'\pm\mathbf{q},\omega'\pm\omega)\times G^0(\mathbf{k}',\omega')G^0(\mathbf{k}'\pm\mathbf{Q},\omega'\pm\Omega). \tag{14}$$

It is straightforward to show, using transformations such as $(\mathbf{k}',\omega')\to(\mathbf{k}'+\mathbf{q},\omega'+\omega)$ and $\mathbf{k}',\mathbf{Q}\to-\mathbf{k}',-\mathbf{Q}$, that the quantum corrections $\phi^{(a),(b),(c)}$ are symmetric in the $\mathbf{q},\omega$ space:

$$\phi(-\mathbf{q},-\omega) = \phi(\mathbf{q},\omega) = \phi(-\mathbf{q},\omega). \tag{15}$$

IV. RESULTS AT HALF-FILLING

In this section, we present results at half-filling for the order-$1/\mathcal{N}$ contributions $\phi^{(a),(b),(c)}$ in the static limit and discuss the evolution of the static magnetic response with increasing interaction strength U. Evaluation of the fermion energy-momentum integrals for the three- and four-fermion vertices [Eqs. (8), (11), and (14)], corresponding to integrating out the fermion degrees of freedom, is illustrated in Appendix A. In our numerical calculations for $\phi^{(a),(b),(c)}$, we have taken grid sizes $dk'=dQ=0.1$, $d\Omega=0.2$, and $\eta=0.1$ on an energy scale $t=1$.

In order to examine the relative contributions to the three quantum corrections $\phi^{(a),(b),(c)}$ from the different internal bosonic modes (involving ladders and bubbles) and the three- and four-fermion vertices $\gamma^{(c)}$ and $\gamma^{(a),(b)}$, we introduce functions $\Gamma^{(a),(b),(c)}(\Omega)$ defined by

$$\phi^{(a),(b),(c)} = \frac{1}{W}\int_{-\infty}^{\infty}d\Omega\Gamma^{(a),(b),(c)}(\Omega), \tag{16}$$

where W is the fermion bandwidth. The functions $\Gamma(\Omega)$ effectively yield combined density of states of the internal excitations involving the vertex functions and the bosonic modes. Typical plots for $\Gamma(\Omega)/W$ are shown in Fig. 3. The symmetric-Ω behavior provides a numerical check for the calculations. It also shows that the intermediate- and high-Ω contributions are quite significant and comparable to the low-Ω contributions which show the usual sharp paramagnon enhancement.

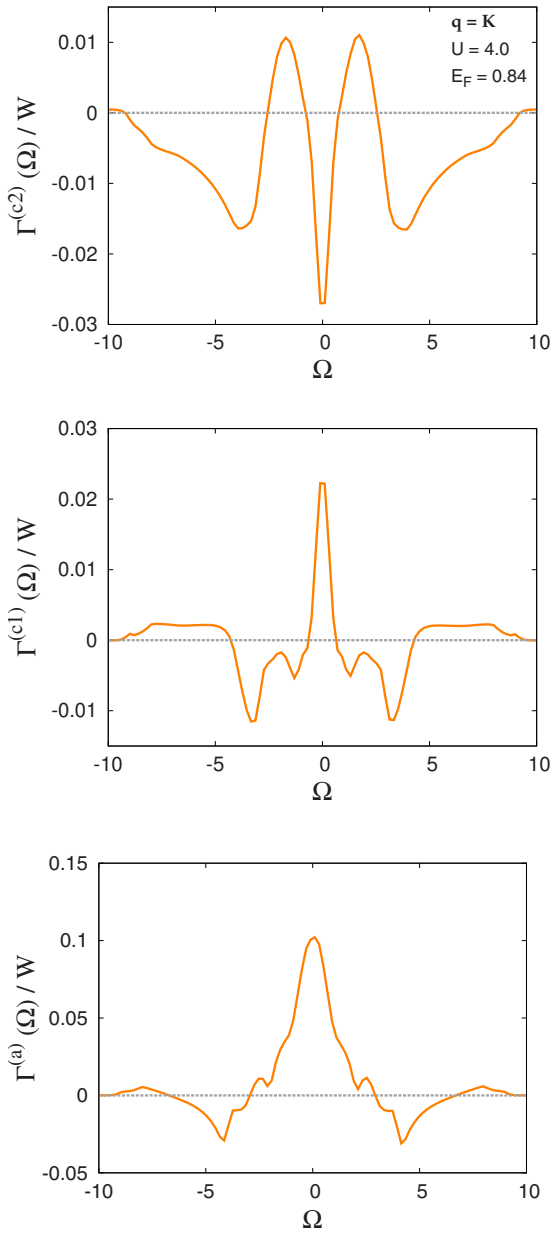

FIG. 3. (Color online) The Ω-resolved contributions of $\phi^{(c_2)}$, $\phi^{(c_1)}$, and $\phi^{(a)}$, showing enhanced contributions at low frequency (paramagnon enhancement) as well as at intermediate and high frequencies.

The Ω-resolved contribution of $\phi^{(c)}$ with only the leading, second-order (U^2) term in Eq. (13) is also shown in Fig. 4(a) for comparison. Apart from the missing low-Ω paramagnon enhancement as expected, it strongly resembles the Ω structure of the full $\phi^{(c_2)}$, implying an essentially fermionic origin for the intermediate- and high-energy structures. Also shown [Fig. 4(b)] is a comparison of the **q** dependence of $\phi^{(c)}$ with the second-order result. Exactly the same **q** structure implies that the fermionic terms $\gamma^{(c)}$ are fully responsible for the characteristic momentum dependence as well. Renormalization of the internal paramagnon mode, within a self-consistent approach, is therefore not expected to qualitatively change this **q** structure.

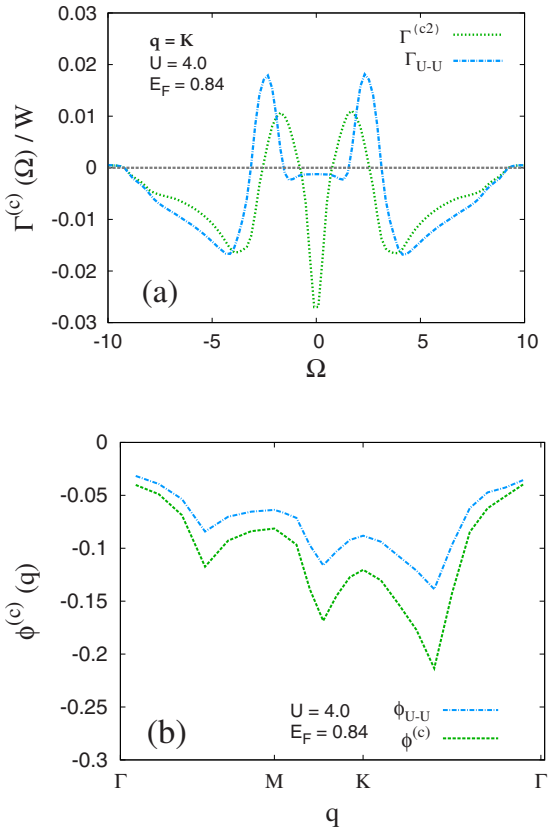

FIG. 4. (Color online) Comparison of $\phi^{(c)}$ with the second-order result, with respect to (a) the Ω-resolved contribution and (b) the **q** dependence.

Evolution of the different contributions $\phi^{(a)}$, $\phi^{(b)}$, and $\phi^{(c)}$ with increasing interaction strength U is shown in Fig. 5, along with their relative comparison for U=4. An enhanced negative contribution of $\phi^{(b)}$ and $\phi^{(c)}$ is seen to occur at the same **q** points where $\chi^0(\mathbf{q})$ peaks. It should also be noted that although the self-energy contribution [Fig. 5(b)] has similar momentum dependence, the largest contribution comes from

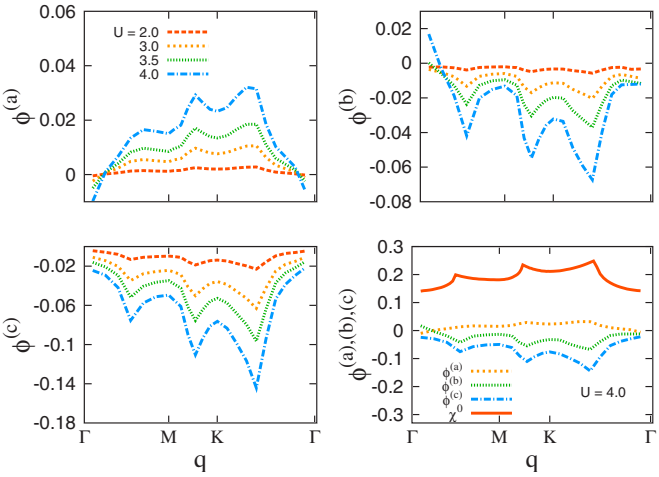

FIG. 5. (Color online) Evolution of the different contributions $\phi^{(a)}$, $\phi^{(b)}$, and $\phi^{(c)}$ with U, showing enhanced negative contribution of $\phi^{(b)}$ and $\phi^{(c)}$ at the same **q** points where $\chi^0(\mathbf{q})$ peaks.

the vertex correction [Fig. 5(c)]. Furthermore, the relative difference between the K and peak contributions is significantly enhanced as compared to that in χ^0. The two diagrams shown in Fig. 2(c_2) at second order in interaction, with a single interaction line in both the ladder sum and the even bubble sum, involve two crossed interaction lines with interactions $U_1=U_2=U$, and, hence, are degenerate for the Hubbard model. Similarly, there is no distinction between the ladder self-energy [Fig. 2(b_1)] and the bubble self-energy [Fig. 2(b_2)] terms at second order. In order to make contact with the single-orbital Hubbard model, this double counting at the U^2 level was, therefore, removed in the calculations of Fig. 5.

We now incorporate, within an approximate resummation scheme,[13] higher order contributions in $1/\mathcal{N}$ to the irreducible propagator ϕ, which become important at intermediate coupling when the first-order quantum correction $\phi^{(1)}(\mathbf{q})$ (which is negative) becomes comparable to the bare response function $\chi^0(\mathbf{q})$. We first note that the characteristic momentum dependence of $\phi^{(1)}(\mathbf{q})$ can be expressed as $\chi^0(\mathbf{q})\alpha\chi^0(\mathbf{q})$, where α is weakly momentum dependent. In this form, the two $\chi^0(\mathbf{q})$ terms can be clearly identified with the pair of particle-hole propagators at either ends of the quantum correction diagrams such as vertex corrections in Fig. 2(c_2) which yield the dominant contribution.

Now, we consider the class of higher order irreducible diagrams with *repeated* $1/\mathcal{N}$ diagrammatic structures, separated by additional $\mathbf{q}$-dependent particle-hole terms. These diagrams involve the maximum number of $\mathbf{q}$-dependent particle-hole terms, and, therefore, yield the dominant $\mathbf{q}$ dependence. The second-order term, e.g., with three such particle-hole propagators, will yield a contribution $\approx\chi^0\alpha\chi^0\alpha\chi^0=\phi^{(1)}[\chi^0]^{-1}\phi^{(1)}$. Summing over this class of diagrams, we approximately obtain the irreducible propagator as

$$\phi(\mathbf{q}) = \frac{\chi^0(\mathbf{q})}{1-\phi^{(1)}(\mathbf{q})/\chi^0(\mathbf{q})}. \tag{17}$$

In order to investigate the U-evolution of the full static magnetic response, we have evaluated the irreducible propagator within the above approximate resummation scheme which allows interpolation into the intermediate-coupling regime. We note here that the approximate Eq. (17) continues to preserve the Goldstone mode in the broken-symmetry state. As the Goldstone mode is exhausted by the lowest-order term χ^0 itself, the quantum correction $\phi^{(1)}$ must identically vanish for $q,\omega=0$, yielding the same result as Eq. (4).

Figure 6, which summarizes the main result of this paper, shows the evolution of $\phi(\mathbf{q})$ with increasing U. The enhanced negative contribution of the quantum corrections $\phi^{(b)}$ and $\phi^{(c)}$—at the same $\mathbf{q}$ points where the bare response $\chi^0(\mathbf{q})$ peaks—results in an inversion of the curvature around K and M with increasing U. The net response is maximum at K, indicating stabilization of the 120°-ordered AF state in the strong-coupling limit. This is consistent with the consensus of a 120°-ordered AF ground state for the equivalent $S=1/2$, nearest-neighbor QHAF on a triangular lattice.[29–33]

In view of the locally maximum renormalized magnetic response at the M point, which is comparable to that at K, it

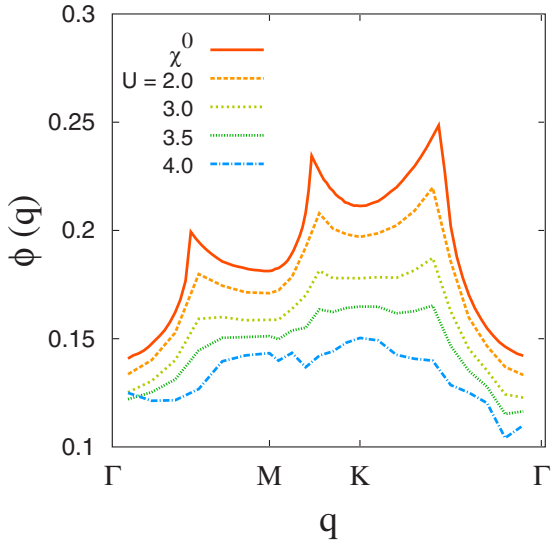

FIG. 6. (Color online) Evolution of the magnetic response function $\phi(\mathbf{q})$ with U, showing the inversion of the curvature around K and M with increasing U, with maximum response at K indicating stabilization of the 120°-ordered AF state in the strong-coupling limit.

is interesting to note that a π-flux spin-liquid state, which on spinon condensation leads to ordering wave vector on the Brillouin zone edge centers (M points), has been proposed for the J-J' QHAF on the triangular lattice.[36]

The change in the curvature of the response function with increasing U implies that it goes through a regime of nearly flat magnetic response around K, as seen in Fig. 6. This is in agreement with the observed lack of dispersion in recent PIRG calculations, where the NMI state has been suggested to be a new type of degenerate quantum spin phase having gapless and dispersionless (flat) spin excitations, indicating a high momentum degeneracy and accounting for the quantum melting of simple translational symmetry breakings including the AF long-ranged order.[26]

This evolution of the magnetic response function highlights a complex feature of correlation effects on magnetic frustration in the triangular-lattice Hubbard model. Initially, increasing interaction strength results in enhanced competing interactions and magnetic frustration, as indicated by the decreasing (negative) curvature of the magnetic response, which even becomes flat in a broad momentum range around K, with the degenerate response indicating high degree of spin disorder. However, beyond a critical interaction strength, the magnetic response develops an increasingly positive curvature around K, indicating build up of 120° AF spin correlations and suppression of magnetic frustration. In the strong-coupling limit, long-range 120° AF order sets in, as only the geometrical frustration of the triangular lattice remains due to the surviving nearest-neighbor AF spin couplings in the equivalent QHAF.

The overall suppression of the magnetic response with increasing U is a manifestation of correlation effects, arising mainly from the particle-particle correlations involved in the vertex correction [Fig. 2(c_2)] with crossed interaction lines and, to a relatively smaller extent, also from the pseudogap

formation due to self-energy corrections [Figs. 2(b_1) and 2(b_2)]. From the PM side, the leading instability toward the 120° AF state at strong coupling and at half-filling is, thus, a consequence of these vertex and self-energy corrections.

The maximum magnetic response at K implies onset of AF spin correlations with short-range 120° ordering. What is the effect of these correlations on the self-energy correction and the electronic density of states? Using characteristic band dispersion identities for the triangular lattice, an approximate analytical estimate for the electron self-energy due to spin-fluctuation scattering yields a two-band structure, with similar dispersion as for the broken-symmetry state, and band separation increasing with interaction strength, eventually leading to the insulating gap.[34]

As the renormalized magnetic response is maximum at K, from Eq. (3) we can estimate the critical interaction strength $U^*=1/\phi(K)\approx 1/0.14\approx 7$ for the magnetic transition to the 120°-ordered AF state. In this estimation, we have assumed that the renormalized *internal* bosonic excitations have the simple form $\chi(\mathbf{Q},\Omega)=\frac{\chi^0(\mathbf{Q},\Omega)}{1-U'\chi^0(\mathbf{Q},\Omega)}$, as considered within the TPSC approximation,[35] with the renormalized interaction $U'\gtrsim 4$ corresponding to the maximum bare response $\chi^0 \lesssim 0.25$. This estimate for U^* is in good agreement with the value obtained earlier ($\gtrsim 6$) from the broken-symmetry side by considering the melting of magnetic order due to quantum spin fluctuations in the 120°-ordered AF state.[11]

V. FINITE DOPING

In the preceding section, the renormalized magnetic response at half-filling was shown to be maximum at K, in accord with the consensus that 120° AF ordering is stabilized in the strong-coupling limit. In this section, we will examine the effects of finite hole and electron doping on the magnetic response function, and, therefore, on the stability of the 120° ordered AF state. Earlier studies have shown that the 120°-ordered AF state is stabilized for hole doping and the spin stiffness is enhanced, whereas it is destabilized for any amount of electron doping.[11] These studies were carried out in the broken-symmetry state, with doped holes and electrons introduced in the AF bands within a rigid-band approximation, and effects of finite doping on transverse spin fluctuations were examined by including the *intraband* particle-hole processes in the particle-hole propagator.

Figure 7 shows a comparison of the bare and renormalized magnetic response for $E_F=-1.0$ (hole doping) and $U=4$. The bare magnetic response shows a pronounced peak at K corresponding to 120° AF ordering, indicating drastic suppression of frustration. We find that since quantum corrections are significantly suppressed, this feature survives at the renormalized level, indicating that the dominant magnetic instability at K remains unchanged.

On the other hand, for electron doping, we find a subtle inversion of the magnetic response near K on a *small-momentum scale*, as shown in Fig. 8(a), indicating destabilization with respect to long-wavelength fluctuations *about* the

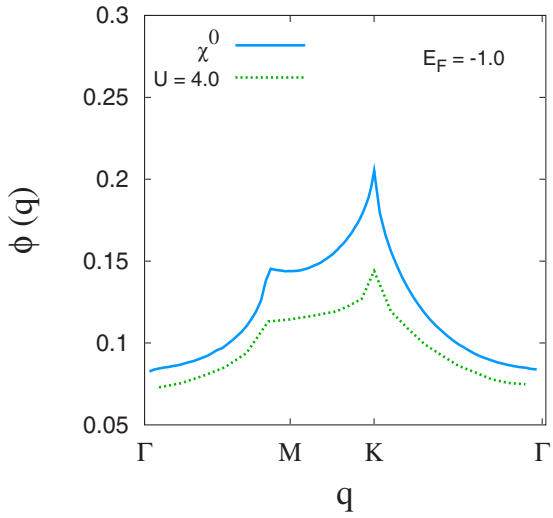

FIG. 7. (Color online) The renormalized magnetic response function $\phi(\mathbf{q})$ for $U=4.0$ and hole doping ($E_F=-1.0$) along with the bare response function $\chi^0(\mathbf{q})$, showing that the maximum response remains at K, corresponding to 120° AF ordering.

120° ordering, in agreement with earlier results.[11] We emphasize that although the bare magnetic response also shows a negative curvature around K, indicating relative instability of the 120°-ordered state, the quantum correction introduces a negative curvature on a much smaller momentum scale. Figure 8(b) shows that this small-momentum feature arises from the self-energy term in $\phi^{(b)}$, and is completely absent in the vertex correction $\phi^{(c)}$.

VI. CONCLUSIONS

In conclusion, we have investigated correlation effects on magnetic frustration in the paramagnetic state of the triangular-lattice Hubbard model. We addressed the question of how the static magnetic response function evolves with increasing interaction strength. This question is important because, whereas the response function at half-filling must peak at the K point $(2\pi/3, 2\pi/\sqrt{3})$ corresponding to the 120° AF ordering expected at strong coupling, it instead exhibits a local minimum at K in the weak-coupling limit. For this purpose, a systematic inverse-degeneracy expansion scheme was employed, which preserves the continuous spin-rotation symmetry and can, therefore, be seamlessly interpolated into the spontaneously-broken-symmetry state at strong coupling, where it will explicitly preserve the Goldstone mode and, hence, allow for study of quantum corrections to spin-wave excitations. First-order quantum corrections, incorporating correlation effects in the form of self-energy and vertex corrections, were numerically evaluated at half-filling as well as at finite electron and hole doping.

At half-filling, our study showed that the nascent 120° AF ordering in the triangular lattice is quantum stabilized. It is only when quantum corrections are incorporated that the magnetic response function at strong coupling peaks at the K point, consistent with the expected onset of 120° AF correlations and eventual instability. In contrast, for the unfrus-

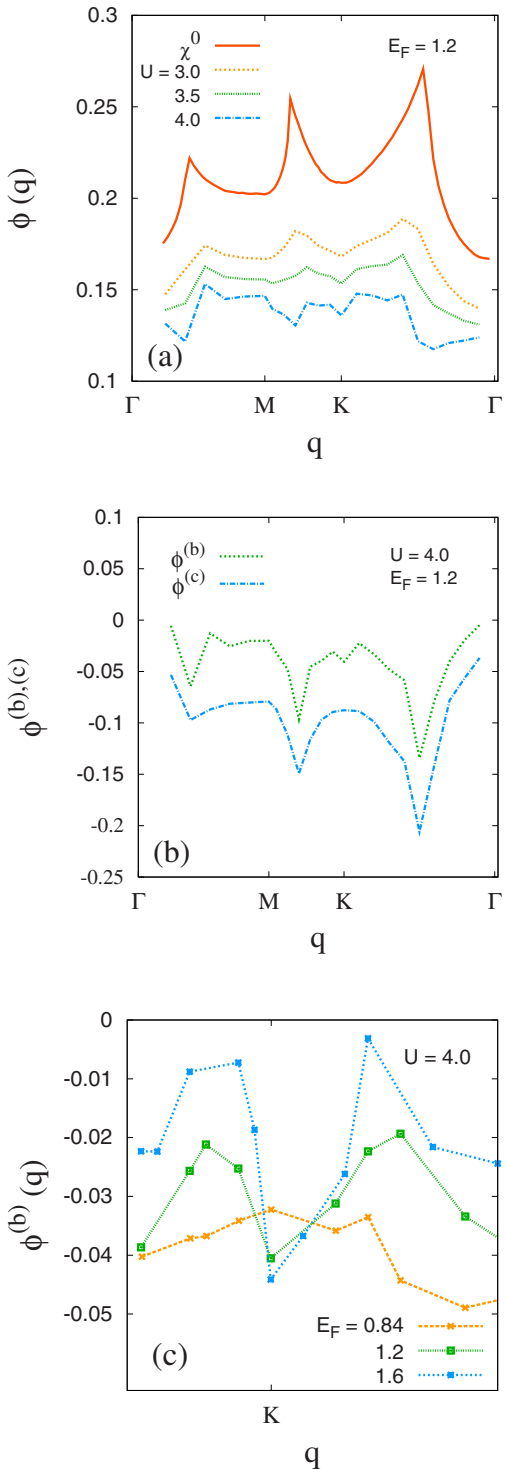

FIG. 8. (Color online) (a) Evolution of $\phi(\mathbf{q})$ with U for the electron-doped case shows a dip near K, indicating destabilization of the 120°-ordered state on a small-momentum scale; (b) this small-momentum feature near K originates from the self-energy contribution $\phi^{(b)}$ and not from the vertex correction $\phi^{(c)}$; (c) A close-up view of this small-momentum feature near K.

trated square lattice, the 180° AF ordering is signalled at the bare level itself, as the bare magnetic response function peaks at the corresponding momentum (π,π). Indeed, the divergent magnetic response at (π,π) in the case of nesting yields antiferromagnetism as a weak-coupling phenomenon.

In renormalizing the magnetic response as above, the dominant quantum correction came from vertex corrections involving crossed interaction lines representing particle-particle correlations. On the other hand, the qualitatively similar but relatively smaller negative self energy contribution reflects suppression of magnetic response due to opening of the pseudo gap. The relative magnitudes highlight the importance of including vertex corrections within the spin-rotationally symmetric approach. The overall suppression of the magnetic response due to the negative contribution of quantum corrections shifts the magnetic transition to higher interaction strength, as expected of quantum fluctuations. We also showed that the fermion terms are responsible for the characteristic momentum behavior of the quantum corrections. Renormalization of the internal paramagnon mode within a self-consistent approach will, therefore, not qualitatively change this momentum behavior.

Our study also provided insight into the evolution of competing interactions and magnetic frustration. We showed that magnetic frustration in the triangular lattice peaks at intermediate coupling. This is seen in the evolution of the magnetic response function near K, which evolves from a concave behavior at weak coupling, through a nearly flat, degenerate response at intermediate coupling, and to a convex behavior at strong coupling. The nearly flat, degenerate response in momentum space near K implies short-range AF spin correlations, suggesting spin-liquid behavior. While only geometric frustration is present at strong coupling due to the nearest-neighbor spin interaction in the equivalent QHAF, the additional extended-range spin interactions generated at intermediate coupling are responsible for the enhanced frustration. A similar picture of enhanced frustration at intermediate coupling was seen earlier from the AF side; with decreasing interaction strength, both the spin stiffness and the magnon energy ω_M at the M point were found to vanish at intermediate coupling, indicating instability of the 120° AF state due to competing interactions.

Electron and hole doping effects were also investigated with respect to the 120° AF instability. For finite electron doping, the response function exhibited a deeper concave behavior around K at weak coupling, and evolved into a nearly degenerate response over a broad momentum range, indicating substantially enhanced frustration. Furthermore, a small-momentum feature in the form of a dip was obtained in the magnetic response function near K, corresponding to instability of the 120° ordering with respect to long-wavelength fluctuations. On the other hand, hole doping was shown to suppress competing interaction and frustration effects, resulting in enhancement of the 120° AF ordering. These results at half-filling and at finite doping are in agreement with earlier results obtained in the AF state.

A self-consistent analysis for both the irreducible particle-hole propagator and the self-energy, incorporating the 120° AF spin correlations in the renormalized internal bosonic modes $(\mathbf{Q},\Omega)$, will highlight the effects of these correlations on dynamical features such as the spin-fluctuation energy

scale, the spectral function $\Im\chi^{-+}(\mathbf{q},\omega)$ of magnetic excitations, the integrated weight of which yields the local spin correlations $\langle S^- S^+ \rangle$ and local moments in the paramagnetic state, as well as the spin-fluctuation self-energy and pseudogap formation in the electronic density of states. Extension of the present work to finite frequencies will, therefore, be of interest in order to study these important dynamical aspects.

APPENDIX A: EVALUATION OF THE THREE-FERMION VERTEX

We illustrate here the evaluation of the fermion terms by integrating out the fermion energy-momentum degrees of freedom for the three-fermion vertex. Including all possible retarded and/or advanced cases, we obtain

$$\begin{aligned}
\gamma^{(c)+}(\mathbf{Q},\Omega) &= i\int_{-\infty}^{\infty}\frac{d\omega'}{2\pi}\sum_{\mathbf{k}'} G^0(\mathbf{k}'+\mathbf{q},\omega'+\omega)G^0(\mathbf{k}',\omega')G^0(\mathbf{k}'+\mathbf{Q},\omega'+\Omega) \\
&= i\int_{-\infty}^{\infty}\frac{d\omega'}{2\pi}\sum_{\mathbf{k}'}\frac{1}{\omega'+\omega-\epsilon^{\pm}_{\mathbf{k}'+\mathbf{q}}\pm i\eta}\frac{1}{\omega'-\epsilon^{\pm}_{\mathbf{k}'}\pm i\eta}\frac{1}{\omega'+\Omega-\epsilon^{\pm}_{\mathbf{k}'+\mathbf{Q}}\pm i\eta} \\
&= i^2\sum_{\mathbf{k}'}\frac{1}{\epsilon^{-}_{\mathbf{k}'+\mathbf{q}}-\epsilon^{+}_{\mathbf{k}'}-\omega+i\eta}\frac{1}{\epsilon^{-}_{\mathbf{k}'+\mathbf{q}}-\epsilon^{+}_{\mathbf{k}'+\mathbf{Q}}+\Omega-\omega+i\eta}+i^2\sum_{\mathbf{k}'}\frac{1}{\epsilon^{-}_{\mathbf{k}'}-\epsilon^{+}_{\mathbf{k}'+\mathbf{q}}+\omega+i\eta}\frac{1}{\epsilon^{-}_{\mathbf{k}'}-\epsilon^{+}_{\mathbf{k}'+\mathbf{Q}}+\Omega+i\eta} \\
&\quad + i^2\sum_{\mathbf{k}'}\frac{1}{\epsilon^{-}_{\mathbf{k}'+\mathbf{Q}}-\epsilon^{+}_{\mathbf{k}'+\mathbf{q}}-\Omega+\omega+i\eta}\frac{1}{\epsilon^{-}_{\mathbf{k}'+\mathbf{Q}}-\epsilon^{+}_{\mathbf{k}'}-\Omega+i\eta}-i^2\sum_{\mathbf{k}'}\frac{1}{\epsilon^{+}_{\mathbf{k}'+\mathbf{q}}-\epsilon^{-}_{\mathbf{k}'}-\omega-i\eta}\frac{1}{\epsilon^{+}_{\mathbf{k}'+\mathbf{q}}-\epsilon^{-}_{\mathbf{k}'+\mathbf{Q}}+\Omega-\omega-i\eta} \\
&\quad - i^2\sum_{\mathbf{k}'}\frac{1}{\epsilon^{+}_{\mathbf{k}'}-\epsilon^{-}_{\mathbf{k}'+\mathbf{q}}+\omega-i\eta}\frac{1}{\epsilon^{+}_{\mathbf{k}'}-\epsilon^{-}_{\mathbf{k}'+\mathbf{Q}}+\Omega-i\eta}-i^2\sum_{\mathbf{k}'}\frac{1}{\epsilon^{+}_{\mathbf{k}'+\mathbf{Q}}-\epsilon^{-}_{\mathbf{k}'+\mathbf{q}}-\Omega+\omega-i\eta}\frac{1}{\epsilon^{+}_{\mathbf{k}'+\mathbf{Q}}-\epsilon^{-}_{\mathbf{k}'}-\Omega-i\eta}. \qquad \text{(A1)}
\end{aligned}$$

The $\mathbf{k}'$ summations were performed numerically over the triangular-lattice Brillouin zone with a grid size $dk'=0.1$.

APPENDIX B: O(1/$\mathcal{N}$) SELF-ENERGY CORRECTION

In Sec. IV, it was mentioned that the negative contribution of $\phi^{(b)}$ arises from the redistribution of spectral weight due to self-energy corrections. We illustrate here this feature in the renormalized density of states resulting from the first-order $(1/\mathcal{N})$ self-energy correction:

$$\Sigma_{\mathbf{k}}(\omega) = U^2\sum_{\mathbf{Q}}\int\frac{d\Omega}{2\pi}\left[\frac{\chi_0(\mathbf{Q},\Omega)}{1-U\chi_0(\mathbf{Q},\Omega)}+\frac{\chi_0(\mathbf{Q},\Omega)}{1-U^2\chi_0^2(\mathbf{Q},\Omega)}\right]G^0(\mathbf{k}-\mathbf{Q},\omega-\Omega) \qquad \text{(B1)}$$

due to exchange of transverse and longitudinal spin fluctuations, corresponding to ladder and bubble diagrams, respectively. The two (retarded and advanced) contributions to the self energy,

$$\Sigma^R_{\mathbf{k}}(\omega) = U^2\sum_{\mathbf{Q}}\int_0^{\infty}\frac{d\Omega}{\pi}\,\mathrm{Im}[\chi_{\mathrm{total}}(\mathbf{Q},\Omega)]_{\mathrm{R}}\frac{1}{\omega-\Omega-\epsilon^{+}_{\mathbf{k}-\mathbf{Q}}+i\eta} \qquad \text{(B2)}$$

and

$$\Sigma^A_{\mathbf{k}}(\omega) = U^2\sum_{\mathbf{Q}}\int_{-\infty}^{0}\frac{d\Omega}{\pi}\,\mathrm{Im}[\chi_{\mathrm{total}}(\mathbf{Q},\Omega)]_{A}\frac{1}{\omega+|\Omega|-\epsilon^{-}_{\mathbf{k}-\mathbf{Q}}-i\eta}, \qquad \text{(B3)}$$

correspond to the intermediate fermion state $\mathbf{k}-\mathbf{Q}$ lying inside $(-)$ or outside $(+)$ the Fermi surface, and the total spin-fluctuation term $[\chi_{\mathrm{total}}(\mathbf{Q},\Omega)]$ includes both the ladder and bubble contributions. The retarded self-energy $\Sigma^R_{\mathbf{k}}(\omega)$ yields negative imaginary part only for $\omega > E_F$, whereas the advanced self-energy $\Sigma^A_{\mathbf{k}}(\omega)$ yields positive imaginary part only for $\omega < E_F$.

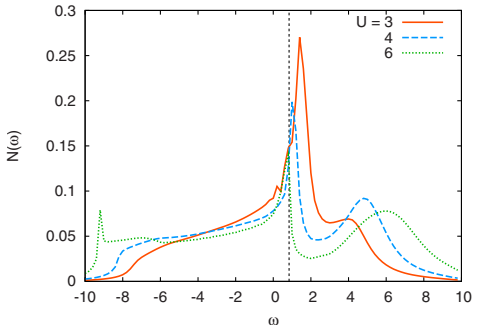

FIG. 9. (Color online) Evolution of the renormalized density of states evaluated from Eq. (B5), showing the opening of the pseudogap with increasing interaction strength U.

The total self-energy $\Sigma_{\mathbf{k}}(\omega)=\Sigma_{\mathbf{k}}^{R}(\omega)+\Sigma_{\mathbf{k}}^{A}(\omega)$ yields the renormalized Green's function:

$$G_{\mathbf{k}}(\omega)=\frac{1}{\omega-\epsilon_{\mathbf{k}}-\Sigma_{\mathbf{k}}(\omega)} \tag{B4}$$

and the one-particle density of states:

$$N(\omega)=\frac{1}{\pi}\sum_{\mathbf{k}}\frac{\mathrm{Im}\,\Sigma_{\mathbf{k}}(\omega)}{[\omega-\epsilon_{\mathbf{k}}-\mathrm{Re}\,\Sigma_{\mathbf{k}}(\omega)]^2+[\mathrm{Im}\,\Sigma_{\mathbf{k}}(\omega)]^2}. \tag{B5}$$

If the intermediate fermion states $\mathbf{k}-\mathbf{Q}$ predominantly lie outside (inside) the Fermi surface for $\mathbf{k}$ inside (outside), as is characteristic of the unfrustrated square lattice for $\mathbf{Q}$ near the AF ordering wave vector (π,π), then the negative (positive) contribution of $\Sigma_{\mathbf{k}}^{R(A)}(\omega)$ pulls down (pushes up) the hole (electron) states in energy, resulting in the opening of an energy gap in the one-particle density of states. Figure 9 shows the emergence of a pseudogap in the renormalized one-particle density of states with increasing interaction strength U.

*gsap@iitk.ac.in

[1] K. Kanoda, Physica C **282-287**, 299 (1997); Hyperfine Interact. **104**, 235 (1997).
[2] R. H. McKenzie, Science **278**, 820 (1997).
[3] K. Takada, H. Sakurai, E. Takayama-Muromachi, F. Izumi, R. A. Dilanian, and T. Sasaki, Nature (London) **422**, 53 (2003).
[4] H. H. Weitering, X. Shi, P. D. Johnson, J. Chen, N. J. Di Nardo, and K. Kempa, Phys. Rev. Lett. **78**, 1331 (1997).
[5] T. Inami, Y. Ajiro, and T. Goto, J. Phys. Soc. Jpn. **65**, 2374 (1996).
[6] L. E. Svistov, A. I. Smirnov, L. A. Prozorova, O. A. Petrenko, L. N. Demianets, and A. Ya. Shapiro, Phys. Rev. B **67**, 094434 (2003).
[7] T. J. Sato, S.-H. Lee, T. Katsufuji, M. Masaki, S. Park, J. R. D. Copley, and H. Takagi, Phys. Rev. B **68**, 014432 (2003).
[8] O. P. Vajk, M. Kenzelmann, J. W. Lynn, S. B. Kim, and S.-W. Cheong, Phys. Rev. Lett. **94**, 087601 (2005).
[9] S. Ghosh and A. Singh, Pramana, J. Phys. **70**, 163 (2008).
[10] T. Chatterji, S. Ghosh, A. Singh, L. P. Regnault, and M. Rheinstädter, Phys. Rev. B **76**, 144406 (2007).
[11] A. Singh, Phys. Rev. B **71**, 214406 (2005).
[12] P. Srivastava and A. Singh, Phys. Rev. B **72**, 224409 (2005).
[13] S.-K. Ma, M. T. Béal-Monod, and D. R. Fredkin, Phys. Rev. **174**, 227 (1968).
[14] A. Singh, Phys. Rev. B **43**, 3617 (1991).
[15] J. A. Hertz and D. M. Edwards, J. Phys. F: Met. Phys. **3**, 2174 (1973).
[16] A. Singh, Phys. Rev. B **74**, 224437 (2006); S. Pandey and A. Singh, *ibid.* **75**, 064412 (2007).
[17] C. J. Gazza, A. E. Trumper, and H. A. Ceccatto, J. Phys.: Condens. Matter **6**, L625 (1994).
[18] M. Capone, L. Capriotti, F. Becca, and S. Caprara, Phys. Rev. B **63**, 085104 (2001).
[19] H. R. Krishnamurthy, C. Jayaprakash, S. Sarker, and W. Wenzel, Phys. Rev. Lett. **64**, 950 (1990); C. Jayaprakash, H. R. Krishnamurthy, S. Sarker, and W. Wenzel, Europhys. Lett. **15**, 625 (1991).
[20] M. Fujita, T. Nakanishi, and K. Machida, Phys. Rev. B **45**, 2190 (1992).
[21] H. Morita, S. Watanabe, and M. Imada, J. Phys. Soc. Jpn. **71**, 2109 (2002).
[22] M. C. Refolio, J. M. López Sancho, and J. Rubio, arXiv: cond-mat/0103459 (unpublished).
[23] S.-W. Tsai and J. B. Marston, Can. J. Phys. **79**, 1463 (2001).
[24] R. Arita, K. Kuroki, and H. Aoki, J. Phys. Soc. Jpn. **73**, 533 (2003).
[25] T. Kashima and M. Imada, J. Phys. Soc. Jpn. **70**, 3052 (2001).
[26] M. Imada, T. Mizusaki, and S. Watanabe, arXiv: cond-mat/0307022 (unpublished); T. Mizusaki and M. Imada, Phys. Rev. B **74**, 014421 (2006).
[27] D. Duffy and A. Moreo, Phys. Rev. B **55**, R676 (1997).
[28] S.-S. Lee and P. A. Lee, Phys. Rev. Lett. **95**, 036403 (2005).
[29] D. A. Huse and V. Elser, Phys. Rev. Lett. **60**, 2531 (1988).
[30] Th. Jolicoeur and J. C. Le Guillou, Phys. Rev. B **40**, 2727 (1989).
[31] B. Bernu, P. Lecheminant, C. Lhuillier, and L. Pierre, Phys. Rev. B **50**, 10048 (1994).
[32] A. V. Chubukov, S. Sachdev, and T. Senthil, J. Phys.: Condens. Matter **6**, 8891 (1994).
[33] L. Capriotti, A. E. Trumper, and S. Sorella, Phys. Rev. Lett. **82**, 3899 (1999).
[34] S. Ghosh and A. Singh (unpublished).
[35] J. Vilk and A.-M. S. Tremblay, J. Phys. I **7**, 1309 (1997).
[36] F. Wang and A. Vishwanath, Phys. Rev. B **74**, 174423 (2006).